

Synthesis, Enhanced Fusogenicity, and Solid State NMR Measurements of Cross-Linked HIV-1 Fusion Peptides[†]

Rong Yang, Jun Yang, and David P. Weliky*

Department of Chemistry, Michigan State University, East Lansing, Michigan 48824

Received October 22, 2002; Revised Manuscript Received January 31, 2003

ABSTRACT: In the HIV-1 gp41 and other viral fusion proteins, the minimal oligomerization state is believed to be trimeric with three N-terminal fusion peptides inserting into the membrane in close proximity. Previous studies have demonstrated that the fusion peptide by itself serves as a useful model fusion system, at least to the hemifusion stage in which the viral and target cell lipids are mixed. In the present study, HIV-1 fusion peptides were chemically synthesized and cross-linked at their C-termini to form dimers or trimers. C-terminal trimerization is their likely topology in the fusogenic form of the intact gp41 protein. The fusogenicity of the peptides was then measured in an intervesicle lipid mixing assay, and the assay results were compared to those of the monomer. For monomer, dimer, and trimer at peptide strand/lipid mol ratios between 0.0050 and 0.010, the final extent of lipid mixing for the dimer and trimer was 2–3 times greater than for the monomer. These data suggest that the higher local concentration of peptide strands in the cross-linked peptides enhances fusogenicity and that oligomerization of the fusion peptide in gp41 may enhance the rate of viral/target cell membrane fusion. For gp41, this effect is in addition to the role of the trimeric coiled–coil structure in bringing about apposition of viral and target cell membranes. NMR measurements on the membrane-associated dimeric fusion peptide were consistent with an extended structure at Phe-8, which is the same as has been observed for the membrane-bound monomer in the same lipid composition.

Membrane fusion plays an essential role in enveloped virus entry into target host cells (1–4). Fusion is mediated by viral envelope proteins that contain apolar fusion peptide domains. The interaction between fusion peptides and lipids is believed to be one key event in initiating membrane fusion (5). Recent studies suggest that fusion protein regions other than the fusion peptide also interact with membranes and play a role in fusion (6–10).

For HIV-1¹ and other enveloped viruses, the free ~20-residue fusion peptide has been shown to be a useful model fusion system, at least to the hemifusion stage in which there is significant mixing between the viral and the target cell lipids. The free peptide causes fusion of liposomes and

erythrocytes, and numerous mutational studies have shown strong correlations between fusion peptide-induced liposome fusion and viral/host cell fusion (5, 11–25).

For both the influenza hemagglutinin and the HIV-1 gp41 envelope proteins, there are crystal and NMR structures of soluble ectodomains in their fusogenic/final fusion conformations (26–32). These trimeric coiled–coil structures represent ~140-residue sequences that begin near the C-terminus of the fusion peptide and end near the N-terminus of the viral transmembrane domain. For the influenza viral fusion protein, a pre-fusion structure has also been observed and is different from the fusogenic/post-fusion coiled–coil structure (26, 32–36). Comparison of these pre- and post-fusion structures suggests movement of the fusion peptide from the interior to the exterior of the protein during fusion so that it can interact with target cell and possibly viral membranes. It is also possible that some of the energy released in the conformational changes is used during fusion. Crystallographic and immunological data suggest that there are also significant structural changes in the HIV-1 fusion proteins during fusion (37, 38).

In the fusogenic coiled–coil structures, the N- and C-terminal ends of the soluble ectodomain are near one another, which implies that fusion peptide and viral transmembrane domains are in close proximity. With the assumption that the fusion peptide is in the target cell membrane, the structures also imply apposition of viral and target cell membranes, which is a reasonable geometry for membrane fusion.

In the present study, we explicitly consider another significant feature implied by the coiled–coil structure: an oligomeric fusion peptide topology with the C-termini of

[†] This work was supported in part by a Camille and Henry Dreyfus Foundation New Faculty Award, by NIH Award R01-AI47153, and NSF Award 9977650 to D.P.W.

* To whom correspondence should be addressed. Telephone: (517) 355-9715. Fax: (517) 353-1793. E-mail: weliky@cem.msu.edu.

¹ Abbreviations: AAA, amino acid analysis; CD, circular dichroism; DMAP, 4-(dimethylamino)pyridine; ESR, electron spin resonance; FID, free induction decay; FMOC, 9-fluorenylmethoxycarbonyl; FP, fusion peptide; FPdm, fusion peptide dimer; FPmn, fusion peptide monomer; FPtr, fusion peptide trimer; FRET, fluorescence resonance energy transfer; HEPES, *N*-2-hydroxyethylpiperazine-*N*'-2-ethanesulfonic acid; HIV, human immunodeficiency virus; HPLC, high-performance liquid chromatography; LM, lipid mixture; LUV, large unilamellar vesicles; MAS, magic angle spinning; NMR, nuclear magnetic resonance; *N*-NBD-PE, *N*-(7-nitro-2,1,3-benzoxadiazol-4-yl)-phosphatidylethanolamine; *N*-Rh-PE, *N*-(lissamine rhodamine B sulfonyl)-phosphatidylethanolamine; PI, phosphatidylinositol; POPC, 1-palmitoyl-2-oleoyl-*sn*-glycero-3-phosphocholine; POPE, 1-palmitoyl-2-oleoyl-*sn*-glycero-3-phosphoethanolamine; POPS, 1-palmitoyl-2-oleoyl-*sn*-glycero-3-[phospho-L-serine]; REDOR, rotational echo double resonance; SDS, sodium dodecyl sulfate; TFA, trifluoroacetic acid; TPPM, two pulse phase modulation.

three fusion peptides in close proximity. The topology has been shown in recent models of membrane fusion (28, 30, 39). Some of these models also consider multiple trimers at the fusion site that would create a high local concentration of fusion peptides (35, 36, 39). In the present study, the C-terminal oligomerization topology was achieved in an HIV-1 fusion peptide model system with cysteine cross-linking.

In most fusion peptide studies to date, the peptides were synthesized as monomers. In membranes, they appear to have considerable structural plasticity and can exist as either monomeric helical or oligomeric β strand or hairpin structures (5, 21–23, 40–52). Recently, a 127-residue FHA2 influenza fusion protein construct was also studied and included both the fusion peptide domain as well as the \sim 100-residue C-terminal of the peptide (6, 53–58). Glutaraldehyde cross-linking showed that this construct is predominantly trimeric in either 2% *n*-octyl β -D-glucoside or 0.5% Triton X-100 detergent. In 2% *n*-octyl β -D-glucoside, cysteine cross-linking studies were consistent with a parallel trimeric arrangement of the helical region C-terminal of the fusion peptide. When a solution of 100 μ M FHA2 in 0.1% Triton was added to a lipid vesicle solution, the induced lipid mixing was significantly higher than that induced by the influenza fusion peptide. In addition, the larger construct induces cell–cell hemifusion. Collectively, these experiments support the hypothesis that an oligomeric topology of the fusion peptide may play a role in fusion.

MATERIALS AND METHODS

Materials. Rink amide resin was purchased from Advanced Chemtech (Louisville, KY), and 9-fluorenylmethoxycarbonyl (Fmoc)-amino acids were obtained from Peptides International (Louisville, KY). 1-Palmitoyl-2-oleoyl-*sn*-glycero-3-phosphocholine (POPC), 1-palmitoyl-2-oleoyl-*sn*-glycero-3-phosphoethanolamine (POPE), 1-palmitoyl-2-oleoyl-*sn*-glycero-3-[phospho-L-serine] (POPS), phosphatidylinositol (PI), sphingomyelin, *N*-(7-nitro-2,1,3-benzoxadiazol-4-yl)-phosphatidylethanolamine (*N*-NBD-PE), and *N*-(lissamine rhodamine B sulfonyl)-phosphatidylethanolamine (*N*-Rh-PE) were purchased from Avanti Polar Lipids, Inc. (Alabaster, AL). The Micro BCA protein assay was obtained from Pierce (Rockford, IL). *N*-2-Hydroxyethylpiperazine-*N'*-2-ethanesulfonic acid (HEPES) and Triton X-100 were obtained from Sigma. All other reagents were analytical grade.

Peptides. Monomer peptides are denoted as FPmn. Several different constructs were synthesized: FP (AVGIGALFLGFLGAAGSTMGARS), FPW (AVGIGALFLGFLGAA-GSTMGARSW), FPK3 (AVGIGALFLGFLGAAGSTMGARSKKK), FPCK3 (AVGIGALFLGFLGAAGSTMGAR-SCKKK), FPCK3 (AVGIGALFLGFLGAAGSTMGAR-SCKKK), FPK3W (AVGIGALFLGFLGAAGSTMGAR-SKKKW), FPCK3W (AVGIGALFLGFLGAAGSTMGAR-SCKKKW), and FPCK3W (AVGIGALFLGFLGAAGSTMGAR-SCKKKW). These peptides were synthesized as their C-terminal amides using a peptide synthesizer (ABI 431A, Foster City, CA) equipped for Fmoc chemistry. The sequences all contain the 23 N-terminal residues of the LAV_{1a} strain of HIV-1 gp41 and were sometimes followed by cysteine(s) for cross-linking and/or three lysines for enhanced solubility and/or a tryptophan as a UV/vis chromophore (59).

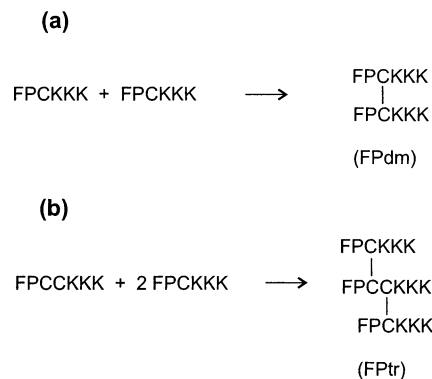


FIGURE 1: Reaction schemes for synthesis of fusion peptide (a) dimers and (b) trimers. The cross-linking was carried out at pH 8.2, and the products were purified by reversed-phase HPLC. FP corresponds to the 23 N-terminal residues of HIV-1 gp41 (LAV_{1a} strain). C and K represent cysteine and lysine residues, respectively.

Peptides were cleaved from the resin in a 3-h reaction using a mixture of TFA/H₂O/phenol/thioanisole/ethanedithiol in a 33:2:2:2:1 volume ratio. Peptides were subsequently purified by reversed-phase HPLC using a preparative C₁₈ column (Vydac, Hesperia, CA) and a water/acetonitrile gradient containing 0.1% TFA. Mass spectroscopy was used to verify peptide purity. Isotopically labeled forms of the peptides were also synthesized with a ¹³C carbonyl label at Phe-8 and a ¹⁵N label at Leu-9.

Cross-Linking. Figure 1 displays the cross-linking reaction schemes. Peptides at \sim 5 mM concentration were cross-linked in 10 mM pH 8.2 DMAP buffer that was open to the atmosphere. Cross-linking was completed within 1 day. FPdm dimers were formed in a solution containing monocysteine peptide, and FPtr trimers were formed in a solution containing dicysteine peptide and monocysteine peptide in a 1:4 mol ratio. Cross-linked peptides of different masses were separated by reversed-phase HPLC with higher mass peptides eluting at higher acetonitrile concentrations. Cross-linked peptide masses were checked using SDS gels and mass spectrometry. For the peak identified as FPtr, greater purity was achieved with a second reversed-phase HPLC purification.

Lipid Preparation. A LM3 lipid/cholesterol mixture was used, which approximately reflects the lipid headgroup and cholesterol composition of the HIV-1 virus and its target T-cells (46, 60). The LM3 mixture had POPC, POPE, POPS, sphingomyelin, PI, and cholesterol in a 10:5:2:2:1:10 mol ratio. Lipid and cholesterol powders were dissolved together in chloroform. The chloroform was removed under a stream of nitrogen followed by overnight vacuum pumping. Lipid dispersions were formed by addition of 5 mM pH 7.0 HEPES buffer containing 0.01% NaN₃ followed by homogenization with 10 freeze–thaw cycles. Large unilamellar vesicles (LUV) of 100-nm diameter were prepared by extrusion (61).

Peptide Concentration Quantitation. Peptide concentrations were quantitated in three different ways: (1) BCA assay; (2) 280-nm absorbance; and (3) quantitative amino acid analysis (AAA). The calibration of the BCA assay was done by comparison with weights of FP. Reproducibility of the BCA assay is \pm 10%. Quantitation from 280 nm absorbance was made using an extinction coefficient of 6000 M⁻¹ cm⁻¹ for FPmn (FPK3W), 12200 M⁻¹ cm⁻¹ for FPdm (made from cross-linking FPK3W) and 7200 M⁻¹ cm⁻¹ for FPtr (made from cross-linking FPCK3W and FPCK3).

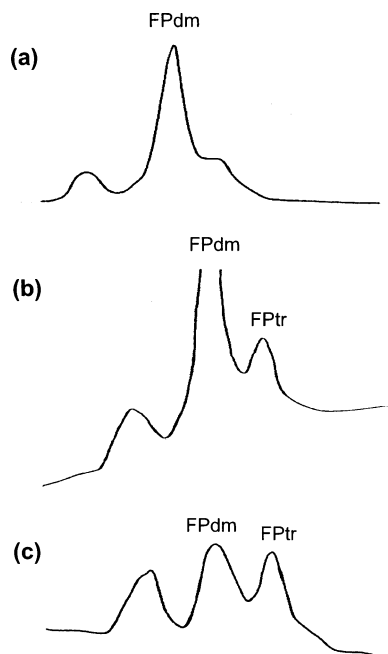


FIGURE 2: HPLC chromatograms of cross-linking reactions. (a) 280-nm detected chromatogram of cross-linking of FPCK3W. The main product is the cross-linked FPdm dimer. (b) 220-nm detected and (c) 280-nm detected chromatograms of cross-linking of FPCK3W and FPCK3 at 1:4 mol ratio. In panel b, the large peak that goes off-scale corresponds to cross-linked FPdm, and the following peak corresponds to cross-linked FPTr trimers. In panel c, the FPTr and FPdm peaks have comparable intensities because at 280 nm, all FPTr is detected whereas only FPdm with at least one FPCK3W strand is detected. For panels a–c, the beginning and end of the chromatograms correspond to 66 and 82% acetonitrile, respectively.

The reproducibility of an absorbance measurement was ± 0.010 or typically $\pm 2\%$. When 280-nm absorbance gave FPmn, FPdm, and FPTr concentrations of 100, 50, and 25 μM , respectively, AAA typically gave concentrations of ~ 90 , 40, and 20 μM , respectively. Because AAA was considered to be the most accurate technique for absolute quantitation, concentrations determined by 280-nm absorbance for FPmn, FPdm, and FPTr solutions were multiplied by 0.9, 0.8, and 0.8, respectively. As will be presented in Figure 3 and Table 1, similar fusion results were obtained when peptide was quantified by AAA and by the BCA assay.

Lipid Mixing Assay for Membrane Fusion. The resonance energy transfer (RET) assay of Struck et al. was used to monitor membrane fusion (62). Two types of 100-nm diameter LM3 LUV were prepared. One set contained 2 mol % of the fluorescent lipid *N*-NBD-PE and 2 mol % of the quenching lipid *N*-Rh-PE, while the other set only contained unlabeled lipids. Fluorescently labeled and unlabeled vesicles were mixed in a 1:9 ratio. Following addition of peptide, lipid mixing between labeled and unlabeled vesicles caused dilution of the labeled lipids with a resulting increase of fluorescence. Fluorescence was recorded using 4-nm bandwidth on an Instruments S. A. Fluoromax-2 (Edison, NJ) spectrofluorimeter operating at excitation and emission wavelengths of 465 and 530 nm, respectively. A siliconized glass cuvette was used with continuous stirring in a thermostated cuvette holder. Measurements were carried out at 37 $^{\circ}\text{C}$ with 2 mL of 150 μM lipid LUV in 5 mM pH 7 HEPES buffer. Peptide solution with initial concentration between 20 and 500 μM was added to the liposome solution

to achieve the desired peptide/lipid mol ratio, and the change in fluorescence of the sample was monitored following this addition. The initial residual fluorescence intensity, F_0 , referenced zero lipid mixing. After addition of peptide, the fluorescence $F(t)$ was monitored as a function of time (t). The maximum fluorescence intensity, F_{max} , was obtained following addition of 20 μL of 10% Triton X-100. Percent lipid mixing at time t is denoted as $M(t)$ and was calculated using

$$M(t) = [(F(t) - F_0)/(F_{\text{max}} - F_0)] \times 100 \quad (1)$$

When the peptide or Triton solution is added to the liposome solution, there are two competing effects on fluorescence: (1) increase because of lipid mixing and (2) decrease because of larger solution volume and corresponding lower fluorophore concentration. The largest added peptide solution volume was 60 μL , which increased the liposome solution volume by 3%. Experimentally, a 3% decrease in fluorescence was also observed when 60 μL of pure buffer was added to the liposome solution. In calculating $M(t)$, $F(t)$ and F_{max} values were adjusted to take into account the small volume changes that occur upon addition of peptide and detergent. With sufficient time, $M(t)$ reached a constant value that is denoted as M_f , the final extent of lipid mixing. M_f was used as a measure of peptide fusogenicity.

To make meaningful comparisons between the lipid mixing abilities of different peptides, the following protocols were developed: (1) the same sets of unlabeled and labeled liposomes were used for all of the peptides in each fusion assay; (2) peptide concentrations were adjusted so that the same volume of each peptide was added for a given peptide strand/lipid ratio; and (3) for each peptide and peptide strand/lipid, two runs were made. The M_f values for the two runs were usually within 2% of each other. The stock peptide solution concentrations varied between 20 and 900 μM , and M_f appeared to be concentration-independent within this range. For most runs, peptide concentrations were ~ 90 μM for FPmn, ~ 40 μM for FPdm, and ~ 20 μM for FPTr.

Solid State NMR Sample Preparation. Between 0.2 and 0.4 μmol of peptide was dissolved in ~ 30 mL of 5 mM HEPES buffer (pH 7) that also contained 0.01% NaN_3 . LUV of LM3 (40 μmol of lipid) were prepared in ~ 5 mL of buffer. The vesicle and peptide solutions were mixed and sat overnight at room temperature. The peptide/lipid mixtures were then ultracentrifuged at 100000g for 4 h so that the membrane and associated peptide pelleted. Pure FPmn or FPdm peptide solutions did not pellet under these conditions. The peptide/lipid pellet formed after ultracentrifugation was transferred by spatula to a 6-mm diameter magic angle spinning (MAS) NMR rotor.

Solid State NMR Spectroscopy. Chemical shifts were referenced to the methylene carbon resonance of adamantane (38.2 ppm). At room temperature and at 0 $^{\circ}\text{C}$, ^{13}C cross-polarization NMR signals were attenuated, presumably because of slow motion. Hence, measurements were made at -50 $^{\circ}\text{C}$ where the samples are rigid and the ^1H spin-lattice relaxation time is < 1 s. With sufficient signal averaging time, spectra can also be obtained at room temperature and are similar to those observed at -50 $^{\circ}\text{C}$ except that the lines are narrower.

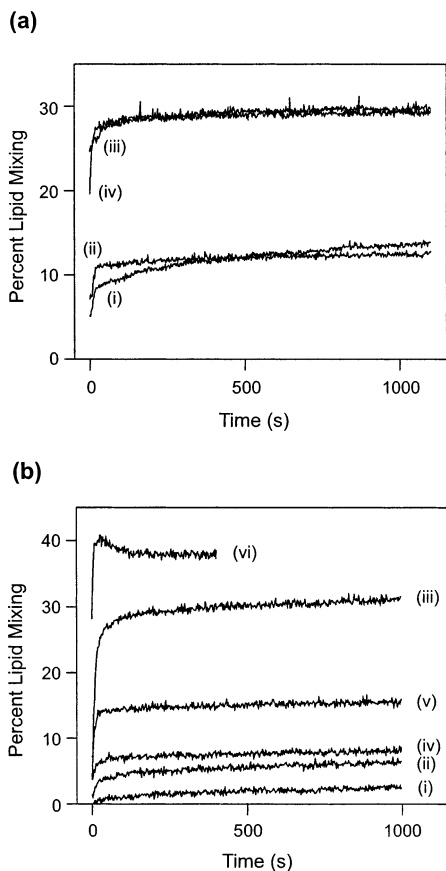


FIGURE 3: Lipid mixing assays. (a) Data for (i) FPmn (FPK3), (ii) FPm (FPCK3), (iii) FPdm (cross-linked product of FPCK3), and (iv) FPtr (cross-linked product of FPCK3 and FPCK3). For lines i–iv, the peptide strand/lipid mol ratio was 0.010, and peptide quantitation was made using the BCA assay. (b) Data for lines i–iii, FPmn (FPK3W) and lines iv–vi, FPdm (cross-linked product of FPCK3W). In lines i and iv, the peptide strand/lipid mol ratio was 0.0050; in lines ii and v, the ratio was 0.010; and in lines iii and vi, the ratio was 0.020. For panel b, peptide quantitation was made by AAA. For all of the runs in panel a, the same sets of liposomes were used, and for all of the runs in panel b, the same sets of liposomes were used.

Experiments were done on a 9.4 T spectrometer (Varian Infinity Plus) using a triple resonance MAS probe. Spacers were placed in the 6-mm rotor so that the sample was restricted to the central 2/3 of the coil length (160 μ L volume), and the ^{13}C and ^{15}N RF fields were reduced by at most 10% from their maximum values in the rotor center. The NMR detection channel was tuned to ^{13}C at 100.8 MHz, the decoupling channel was tuned to ^1H at 400.8 MHz, and the third channel was tuned to ^{15}N at 40.6 MHz. Experiments were carried out using a MAS frequency of 8000 Hz that was stabilized to ± 2 Hz. For the NMR experiments, peptides were ^{13}C carbonyl labeled at Phe-8 and ^{15}N amide labeled at Leu-9. NMR spectra were taken using a REDOR filter of the ^{13}C – ^{15}N dipolar interaction so that the Phe-8 carbonyl was the only signal observed in the ^{13}C -detected REDOR difference spectrum (52, 63). Between 1 and 2 ms of cross-polarization at 50 kHz was followed by a 1-ms REDOR dephasing period and then direct ^{13}C detection. A single 50-kHz ^{13}C refocusing π pulse was placed at the center of the dephasing time, and ^1H TPPM decoupling of 65 kHz was applied during both dephasing and detection (64). The ^{13}C transmitter frequency was set to 155 ppm, and the ^{15}N

frequency was near the isotropic peptide amide resonance. For the S_1 acquisition, the dephasing time contained a 40-kHz ^{15}N π pulse at the middle and end of each rotor period, while the S_0 acquisition did not contain these pulses. XY-8 phase cycling was used for the ^{15}N pulses (65, 66). During the dephasing period, pulses were not actively synchronized to the rotor phase. To obtain optimal compensation of B_0 , B_1 , and spinning frequency drifts, S_0 and S_1 FID values were acquired alternately. The recycle delay was 1 s.

RESULTS

Synthesis and Characterization of Cross-Linked Peptides.

Figure 2a displays the 280-nm detected reversed-phase chromatogram of the products formed by cross-linking of FPCK3W. The main peak corresponds to the FPdm dimer. Peak identification was made by mass spectrometry with supporting evidence that under the same chromatographic conditions, the FPCK3W monomer eluted at lower acetonitrile concentration than FPdm. Figure 2b displays the 220-nm detected chromatogram of the cross-linking products formed from the reaction of FPCK3W and FPCK3 in a 1:4 mol ratio. The largest peak corresponds to FPdm, while the following peak corresponds to the FPtr trimer. Again, this assignment was made by mass spectroscopy. In terms of increasing hydrophobicity, the molecules can be ordered FPmn, FPdm, and FPtr, and this also matches the ordering of the acetonitrile concentration at elution. Additional evidence for the trimer assignment was by made by detection of the chromatogram at 280 nm, as displayed in Figure 2c. In this chromatogram, the FPdm and FPtr peaks have approximately equal intensity. The peak intensities in panels b and c are qualitatively consistent with 220-nm detection of all FPtr and FPdm and 280-nm detection of all FPtr and only FPdm containing at least one FPCK3W strand.

As evidenced in Figure 2a, FPdm was the major product formed in cross-linking of either pure FPCK3W or FPCK3. Using 6 mg of monomer starting material, ~ 3 mg of FPdm could be obtained after HPLC purification. FPtr was not the major product of cross-linking (cf. Figure 2b), and after HPLC purification and repurification, ~ 0.2 mg of FPtr was obtained from a cross-linking reaction that began with 15 mg of monomer starting material.

Analytical ultracentrifugation demonstrated that 75 μM FPK3W is predominantly monomeric in 5 mM pH 7 HEPES buffer. A mixture of monomer and higher order oligomerization states were observed for FPdm and FPtr at concentrations of 30 and 20 μM , respectively.

Fusion of LM3 Vesicles. Figure 3a displays one example of intervesicle lipid mixing induced by FPmn, FPdm, and FPtr at peptide strand/lipid = 0.010. In this case, FPmn was either FPK3 or FPCK3, FPdm was formed from cross-linking of FPCK3, and FPtr was formed from cross-linking of FPCKKKK and FPCKKK in a 1:4 mol ratio. Peptide concentrations were determined by the BCA assay. Because FPdm and FPtr have respectively twice and three times as many strands per molecule as FPmn, the peptide/lipid mol ratios for FPmn, FPdm, and FPtr are 0.010, 0.0050, and 0.0033, respectively. In these data, the M_f values for FPdm and FPtr are about two times greater than the M_f for FPmn. Figure 3b displays more lipid mixing data for FPmn (FPK3W) and FPdm (made from cross-linking FPCK3W).

Table 1: Fusogenicity Ratios as a Function of Peptide Strand/Lipid

Peptide Strand/ Lipid Mol Ratio	Fusogenicity Ratio ^a	
	FPdm/FPmn	FPtr/FPmn
0.0050	2.6 (0.5)	2.2 (0.3)
0.010	2.1 (0.3)	1.9 (0.4)
0.020	1.3 (0.1)	n.d. ^b

^a This is calculated from the ratios of M_f values. The average fusogenicity ratio is followed by its standard deviation in parentheses.
^b Not determined.

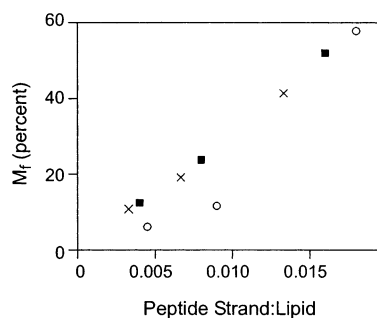


FIGURE 4: Fusogenicity M_f vs peptide strand/lipid mol ratio. Open circles represent data for FPmn (FPK3W), closed squares represent data for FPdm (obtained from cross-linking FPCK3W), and crosses represent data for FPTr (obtained from cross-linking FPCK3W and FPCK3). All of the data were obtained using the same sets of liposomes. The uncertainty in each M_f value is $\pm 1\%$.

In this case, peptide quantitation was made from AAA. At peptide strand/lipid = 0.0050 and 0.010, FPdm has 2–3 times the fusogenicity of FPmn, while at 0.020 ratio, the enhancement factor is about 1.3.

The final extent of lipid mixing, M_f , was used as a general measure of peptide fusogenicity. Figure 4 displays a plot of M_f as a function of peptide strand/lipid mol ratio for assays using FPmn, FPdm, and FPTr with the same sets of liposomes. For these data, FPmn was FPK3W, FPdm was obtained from cross-linking FPCK3W, and FPTr was obtained from cross-linking FPCK3W and FPCK3 in a 1:4 mol ratio. The fusogenicities of FPdm and FPTr are comparable over the experimental range of peptide strand/lipid mol ratios. At lower (≤ 0.010) peptide strand/lipid ratios, FPdm and FPTr are significantly more fusogenic than FPmn while at ratios closer to 0.020, the fusogenicities of the three peptides are much more comparable.

When comparing runs using different sets of liposomes, there can be considerable variation in the M_f values, even for the same peptide and peptide strand/lipid. A more meaningful measure is the ratio of the M_f value of FPdm or FPTr to the M_f value of FPmn. For runs from the same sets of liposomes, these fusogenicity ratios were calculated at peptide strand/lipid mol ratios of 0.0050, 0.010, and 0.020. In some runs, the data had been obtained at peptide strand/lipid different than these three standard values so linear interpolation was used to calculate the fusogenicity ratios at the standard values. There was general consistency in the fusogenicity ratios among different liposome batches as evidenced in Table 1, which displays the average values and standard deviations of the fusogenicity ratios. For example, the FPdm/FPmn fusogenicity ratio at peptide strand/lipid = 0.010 represents the average of measurements taken with six different sets of liposomes. In addition, for a given peptide strand/lipid, the fusogenicity ratio is independent of the

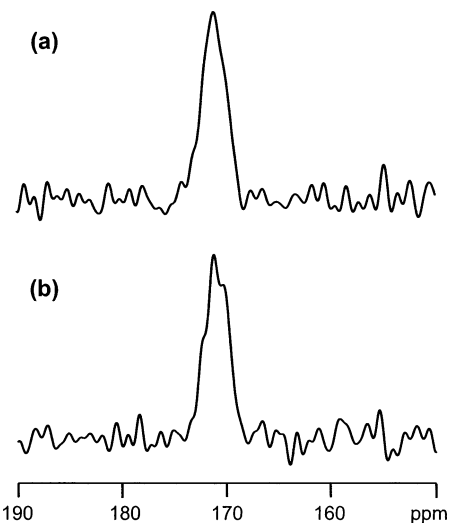


FIGURE 5: ^{13}C NMR spectra of LM3-associated (a) FPmn (FPK3W) and (b) FPdm (obtained from cross-linking FPCK3W). The peptide strand/lipid mol ratio is 0.009 for FPmn and 0.008 for FPdm. The spectra were obtained at -50°C . Each peptide has a ^{13}C carbonyl label at Phe-8 and a ^{15}N label at Leu-9. Because of the REDOR filter, only signals from the Phe-8 carbonyl are observed in the spectra. Each spectrum was processed with 25 Hz line broadening. The FPmn and FPdm spectra represent the co-addition of 93280 and 74480 scans, respectively.

presence or absence of the C-terminal tryptophan in FPmn, FPdm, or FPTr and is also independent of the presence or absence of the cysteine in FPmn (cf. Figure 3a).

Solid State NMR Measurements. Figure 5 displays solid state NMR REDOR difference spectra of LM3-associated FPmn and FPdm at peptide/lipid mol ratios of 0.009 and 0.004, respectively. The FPmn construct was FPK3W, and FPdm was made from cross-linking FPCK3W. Both FPmn and FPdm were ^{13}C carbonyl labeled at Phe-8 and ^{15}N amide labeled at Leu-9, and the REDOR-filtered difference spectra only show signals from the ^{13}C carbonyl labeled Phe-8. The displayed FPmn and FPdm spectra are very similar and have a peak centered at 171 ppm with 2.5 ppm line width (full-width at half-maximum). Similar spectra were obtained for other LM3-associated FPmn constructs including FP, FPK3, and FPW (data not shown). In Figure 5, the FPdm spectrum shows partial resolution of three components, which is not apparent in the displayed FPmn spectrum. However, we have also observed these components in spectra of some other FPmn samples and hence conclude that they are not uniquely related to the FPdm.

Chemical shift correlation tables suggest that a 171 ppm Phe chemical shift is consistent with nonhelical structure (67). In addition, solution NMR has shown that in detergent, FPmn is predominantly helical (40, 68). In frozen detergent, the solid state NMR spectrum of labeled FPmn (FPKKK) yielded a sharp line whose peak chemical shift is 175 ppm (data not shown). In LM3, the peak chemical shift is 4 ppm lower, a difference that provides further evidence for nonhelical structure in LM3. Finally, for FPmn, previous solid state NMR 2-D exchange measurements were also consistent with nonhelical β strand structure at Phe-8 (46).

DISCUSSION

The topology of insertion of the HIV-1 fusion peptide is strongly suggested from high-resolution structures of the

soluble portion of the gp41 ectodomain (27–31). In this topology, the C-termini of three fusion peptides are near one another, and there is the possibility that the fusion peptides insert into the membrane in close proximity. In the present paper, we have synthesized fusion peptides that are cross-linked at their C-termini with a topology close to that found in the full protein. Relative to the monomer peptide, these cross-linked peptides enhance fusogenicity at least to the lipid mixing stage, which suggests that this topology may be a significant structural factor in catalyzing viral/target cell fusion. The studies in this paper consider the final extent of lipid mixing as a measure of fusogenicity, but in the future we also plan to carefully investigate the rates for buildup of lipid mixing. Preliminary analysis shows that these rates are generally larger for cross-linked peptides than for FPmn, and with further analysis and temperature-dependent studies, it may be possible to quantify the effect of topology on the activation energy of membrane fusion.

The enhanced fusogenicities of cross-linked fusion peptides are consistent with the hypothesis that lipid mixing induced by fusion peptides requires some critical local concentration of peptide strands associated with the membrane. For FPdm and FPtr, the local concentration is elevated by cross-linking so that relative to FPmn, the cross-linked peptides allow greater lipid mixing at lower peptide strand/lipid. At higher peptide strand/lipid, FPmn, FPdm, and FPtr would all have surpassed the critical concentration and would have more similar fusion activities, which is consistent with experimental observation (cf. Figure 4 and Table 1). The proposed correlation between local peptide concentration and fusogenicity has some similarity to an earlier hypothesis that fusion requires a critical number of fusion peptides per vesicle (24). However, this latter hypothesis predicts that at constant peptide/lipid, fusion will be greater for larger vesicles, and we observed that for FPmn, M_f is independent of LM3 vesicle size (69).

In addition to the higher local peptide concentration achieved with cross-linking, the overall concentration of cross-linked fusion peptide in LM3 could be higher than that of FPmn because of higher lipid affinity of the cross-linked peptide. However, there is some experimental evidence that points against different affinities of the different peptides. In the absence of LM3, BCA assay measurements showed that neither FPmn nor FPdm pellet under the ultracentrifugation conditions used to make the solid state NMR samples (46). During preparation of FPmn (FP or FPKKK) NMR samples at 10 μ M peptide and 1 mM lipid, BCA data also showed little peptide in the centrifugation supernatant (46, 69). Taken together, these observations suggest quantitative association of FPmn with LM3. In addition, there was approximately the same NMR signal per scan for the FPmn and FPdm samples (cf. Figure 5), which is consistent with comparable (quantitative) membrane binding for both peptides. For samples made under the conditions of the lipid mixing assay (1.5 μ M FPmn or 0.75 μ M FPdm and 150 μ M lipid), peptide binding was not accurately measured because of large background signals in the BCA assay from HEPES and uncentrifuged lipid.

In related studies, other investigators have studied the lipid binding and fusogenicities of peptides that contained between 16 and 70 of the N-terminal residues of gp41 (7, 10). Longer peptides had higher fusogenicities, but at 0.1 μ M peptide

concentration there were negligible differences in the lipid affinities of the different peptides. These data are similar to the different fusogenicities and comparable binding that we observed for FPmn and FPdm.

In more detailed molecular structural picture, there are at least two models that correlate cross-linking with enhanced fusogenicity. In one model, the main effect is greater peptide/lipid interactions that lead to larger membrane disruption. For example, a splayed helix model for oligomers has noninteracting helices that insert obliquely into the membrane (56). In a trimer, each helix forms an edge of a trigonal pyramidal structure.

In a second model, the topology correlates with a particular structural arrangement of interacting peptide strands, perhaps a parallel β sheet structure. For FPmn, solid state NMR measurements have demonstrated that in LM3 at peptide/lipid ≥ 0.010 , the N-terminal and central regions of the peptide adopt a nonhelical β strand structure (46). In Figure 5, the 1-D solid state NMR spectra for the Phe-8 carbonyl are very similar for LM3-associated FPmn and FPdm, which suggests that FPdm also forms a β strand at this residue. Additional solid state NMR REDOR studies have shown that there are both parallel and antiparallel arrangements of strands in LM3-associated FPmn (69). However, the C-terminal cross-linking topology of FPdm and FPtr suggests a parallel arrangement of strands. Furthermore, it is possible that the parallel alignment is more fusogenic than the antiparallel alignment. For the parallel arrangement, the apolar N-terminal regions of two or more peptide strands could insert into the hydrophobic interior of the membrane, which could be more disruptive to the membrane than a single peptide strand. This particular insertion topology is less likely with the antiparallel arrangement in which the polar and apolar ends of strands would be on the same side of the oligomer. Thus, FPmn, which has a mix of both parallel and antiparallel alignments, would be less fusogenic than FPdm and FPtr. The actual strand arrangement of the membrane-associated cross-linked peptides will be investigated by solid state NMR and other experimental methods. It is likely that any structure that inserts into the hydrophobic core of the membrane will require arrangements of strands in which most carbonyl oxygens and amide protons participate in inter- or intrapeptide hydrogen bonds. It is noted that in the solid state NMR experiments, the peptide structure is observed after vesicle fusion has occurred. It is also possible that fusion requires a transient structure that is different from the NMR structure observed at the end state of fusion.

At peptide strand/lipid mol ratios between 0.004 and 0.015, FPdm and FPtr have approximately the same fusogenicity (cf. Figures 3 and 4 and Table 1). This may be a general observation that the dimeric and trimeric topologies have approximately the same effect on lipid mixing. However, it is also noted that FPdm has an in-register strand alignment, whereas FPtr has one strand out of register with the other two strands (cf. Figure 1). In gp41, the three strands are likely in-register, and it is possible that this arrangement is a structural requirement for enhanced fusogenicity. In the future, an in-register FPtr will be synthesized using differential cysteine protection and introduction of a spacer residue in the third strand (70).

Our results suggest that oligomeric fusion peptide topology may have also contributed to the enhanced fusogenicity

observed for the 127-residue FHA2 domain of influenza envelope protein (6, 56, 57) and for the construct containing residues 1–70 of gp41 (10). In these systems, there is likely additional fusogenic enhancement because of the presence of other regions of the fusion protein. For the gp41 system, the overall fusogenicity of the 1–70 construct was about 10 times greater than that of the 1–23 construct, and this is a larger enhancement than we observed from cross-linking the 1–23 construct. In addition, although the 127-residue FHA2 induces cell–cell hemifusion, a 90-residue construct containing the fusion peptide and ~70 C-terminal residues does not induce cell–cell hemifusion (57). One possible explanation for this observation is that the 37 extra residues in FHA2 contain a kinked loop region that is required for pH-dependent association of FHA2 trimers and for cell–cell hemifusion (6, 55, 56, 58).

In this study as well as lipid mixing studies from other groups, it is possible that the oligomerization of peptides in aqueous solution prior to interaction with the target membrane impacts the rate and extent of lipid mixing. For our work, analytical ultracentrifugation demonstrated that FPmn (FPK3W construct) is predominantly a monomer in the assay buffer, whereas FPdm and FPtr are mixtures of monomeric and oligomeric cross-linked peptides. Thus, the possibility exists that some part of the enhanced fusogenicity of FPdm and FPtr is related to their oligomeric state in aqueous solution. However, studies of different FPmn peptide constructs that were either monomeric or oligomeric in aqueous solution did not show a clear correlation between M_r and oligomeric state (69). In addition, for the influenza fusion peptide, there does not appear to be a correlation between the peptide oligomeric state in aqueous solution and its final oligomeric state in the membrane, which suggests that oligomers can break up and/or (re)form at the membrane interface (71). In the future, we plan to specifically address the effect of oligomerization by synthesis of cross-linked fusion peptides with longer C-terminal lysine sequences. Analytical ultracentrifugation of influenza fusion peptides showed that additional lysines could change the peptide from an oligomeric to a monomeric state in solution (data not shown). We expect that a similar effect may also be observed for the cross-linked HIV-1 fusion peptides.

In summary, we have shown a correlation between C-terminal cross-linking and enhanced fusogenicity of HIV-1 fusion peptides. The topology achieved through cross-linking is similar to the fusion peptide topology thought to exist in the fusogenic form of gp41. Thus, the topology may play a role in enhancing membrane fusion rates. The synthetic methodology described in this paper should be generally applicable to fusion peptides from other viruses. Less soluble peptide sequences (such as that from influenza) will require longer C-terminal guest lysine sequences. Because it is possible to obtain these cross-linked peptides in relatively high quantities, it is expected that structural and motional information about them will be readily obtained from techniques such as NMR, ESR, infrared, neutron diffraction, CD, and FRET, etc.

ACKNOWLEDGMENT

We acknowledge Yechiel Shai for pointing out the second structural model as a possible explanation for our data. We

acknowledge the MSU mass spectrometry and macromolecular facilities for assistance with mass spectrometry and quantitative amino acid analysis. We acknowledge Drs. Mary Prorok and Mark Lemmon for the analytical ultracentrifugation data and Dr. Honggao Yan for use of his fluorimeter. We acknowledge Dr. Mary Barkley for suggesting amino acid analysis as a method of peptide quantitation. We thank Charles Gabrys for a critical reading of this paper.

REFERENCES

- Hernandez, L. D., Hoffman, L. R., Wolfsberg, T. G., and White, J. M. (1996) Virus–cell and cell–cell fusion, *Annu. Rev. Cell Dev. Biol.* 12, 627–661.
- Blumenthal, R., and Dimitrov, D. S. (1997) Membrane Fusion, in *Handbook of Physiology, Section 14: Cell Physiology* (Hoffman, J. F., and Jamieson, J. C., Eds.) pp 563–603, Oxford, New York.
- Dimitrov, D. S. (2000) Cell biology of virus entry, *Cell* 101, 697–702.
- Eckert, D. M., and Kim, P. S. (2001) Mechanisms of viral membrane fusion and its inhibition, *Annu. Rev. Biochem.* 70, 777–810.
- Durell, S. R., Martin, I., Ruyschaert, J. M., Shai, Y., and Blumenthal, R. (1997) What studies of fusion peptides tell us about viral envelope glycoprotein-mediated membrane fusion (review), *Mol. Membr. Biol.* 14, 97–112.
- Epand, R. F., Macosko, J. C., Russell, C. J., Shin, Y. K., and Epand, R. M. (1999) The ectodomain of HA2 of influenza virus promotes rapid pH dependent membrane fusion, *J. Mol. Biol.* 286, 489–503.
- Peisajovich, S. G., Epand, R. F., Pritsker, M., Shai, Y., and Epand, R. M. (2000) The polar region consecutive to the HIV fusion peptide participates in membrane fusion, *Biochemistry* 39, 1826–1833.
- Peisajovich, S. G., Samuel, O., and Shai, Y. (2000) Paramyxovirus F1 protein has two fusion peptides: implications for the mechanism of membrane fusion, *J. Mol. Biol.* 296, 1353–1365.
- Suarez, T., Gallaher, W. R., Agirre, A., Goni, F. M., and Nieva, J. L. (2000) Membrane interface-interacting sequences within the ectodomain of the human immunodeficiency virus type 1 envelope glycoprotein: putative role during viral fusion, *J. Virol.* 74, 8038–8047.
- Sackett, K., and Shai, Y. (2002) The HIV-1 gp41 N-terminal heptad repeat plays an essential role in membrane fusion, *Biochemistry* 41, 4678–4685.
- Freed, E. O., Myers, D. J., and Risser, R. (1990) Characterization of the fusion domain of the human immunodeficiency virus type 1 envelope glycoprotein gp41, *Proc. Natl. Acad. Sci. U.S.A.* 87, 4650–4654.
- Freed, E. O., Delwart, E. L., Buchsacher, G. L., Jr., and Panganiban, A. T. (1992) A mutation in the human immunodeficiency virus type 1 transmembrane glycoprotein gp41 dominantly interferes with fusion and infectivity, *Proc. Natl. Acad. Sci. U.S.A.* 89, 70–74.
- Schaal, H., Klein, M., Gehrmann, P., Adams, O., and Scheid, A. (1995) Requirement of N-terminal amino acid residues of gp41 for human immunodeficiency virus type 1-mediated cell fusion, *J. Virol.* 69, 3308–3314.
- Delahunty, M. D., Rhee, I., Freed, E. O., and Bonifacino, J. S. (1996) Mutational analysis of the fusion peptide of the human immunodeficiency virus type 1: identification of critical glycine residues, *Virology* 218, 94–102.
- Pecheur, E., Sainte-Marie, J., Bienvenue, A., and Hoekstra, D. (1999) Peptides and membrane fusion: towards an understanding of the molecular mechanism of protein-induced fusion, *J. Membr. Biol.* 167, 1–17.
- Rafalski, M., Lear, J. D., and DeGrado, W. F. (1990) Phospholipid interactions of synthetic peptides representing the N-terminus of HIV gp41, *Biochemistry* 29, 7917–7922.
- Slepushkin, V. A., Melikyan, G. B., Sidorova, M. S., Chumakov, V. M., Andreev, S. M., Manulyan, R. A., and Karamov, E. V. (1990) Interaction of human immunodeficiency virus (HIV-1) fusion peptides with artificial lipid membranes, *Biochem. Biophys. Res. Commun.* 172, 952–957.
- Martin, I., Defrise-Quertain, F., Decroly, E., Vandenbranden, M., Bresseur, R., and Ruyschaert, J. M. (1993) Orientation and

- structure of the NH₂-terminal HIV-1 gp41 peptide in fused and aggregated liposomes, *Biochim. Biophys. Acta* 1145, 124–133.
19. Nieva, J. L., Nir, S., Muga, A., Goni, F. M., and Wilschut, J. (1994) Interaction of the HIV-1 fusion peptide with phospholipid vesicles: different structural requirements for fusion and leakage, *Biochemistry* 33, 3201–3209.
 20. Mobley, P. W., Lee, H. F., Curtain, C. C., Kirkpatrick, A., Waring, A. J., and Gordon, L. M. (1995) The amino-terminal peptide of HIV-1 glycoprotein 41 fuses human erythrocytes, *Biochim. Biophys. Acta* 1271, 304–314.
 21. Martin, I., Schaal, H., Scheid, A., and Ruyschaert, J. M. (1996) Lipid membrane fusion induced by the human immunodeficiency virus type 1 gp41 N-terminal extremity is determined by its orientation in the lipid bilayer, *J. Virol.* 70, 298–304.
 22. Klinger, Y., Aharoni, A., Rapaport, D., Jones, P., Blumenthal, R., and Shai, Y. (1997) Fusion peptides derived from the HIV type 1 glycoprotein 41 associate within phospholipid membranes and inhibit cell–cell fusion. Structure–function study, *J. Biol. Chem.* 272, 13496–13505.
 23. Pereira, F. B., Goni, F. M., Muga, A., and Nieva, J. L. (1997) Permeabilization and fusion of uncharged lipid vesicles induced by the HIV-1 fusion peptide adopting an extended conformation: dose and sequence effects, *Biophys. J.* 73, 1977–1986.
 24. Nieva, J. L., Nir, S., and Wilschut, J. (1998) Destabilization and fusion of zwitterionic large unilamellar lipid vesicles induced by a beta-type structure of the HIV-1 fusion peptide, *J. Liposome Res.* 8, 165–182.
 25. Pritsker, M., Rucker, J., Hoffman, T. L., Doms, R. W., and Shai, Y. (1999) Effect of nonpolar substitutions of the conserved Phe11 in the fusion peptide of HIV-1 gp41 on its function, structure, and organization in membranes, *Biochemistry* 38, 11359–11371.
 26. Bullough, P. A., Hughson, F. M., Skehel, J. J., and Wiley, D. C. (1994) Structure of influenza haemagglutinin at the pH of membrane fusion, *Nature* 371, 37–43.
 27. Chan, D. C., Fass, D., Berger, J. M., and Kim, P. S. (1997) Core structure of gp41 from the HIV envelope glycoprotein, *Cell* 89, 263–273.
 28. Weissenhorn, W., Dessen, A., Harrison, S. C., Skehel, J. J., and Wiley, D. C. (1997) Atomic structure of the ectodomain from HIV-1 gp41, *Nature* 387, 426–430.
 29. Tan, K., Liu, J., Wang, J., Shen, S., and Lu, M. (1997) Atomic structure of a thermostable subdomain of HIV-1 gp41, *Proc. Natl. Acad. Sci. U.S.A.* 94, 12303–12308.
 30. Caffrey, M., Cai, M., Kaufman, J., Stahl, S. J., Wingfield, P. T., Covell, D. G., Gronenborn, A. M., and Clore, G. M. (1998) Three-dimensional solution structure of the 44 kDa ectodomain of SIV gp41, *EMBO J.* 17, 4572–4584.
 31. Yang, Z. N., Mueser, T. C., Kaufman, J., Stahl, S. J., Wingfield, P. T., and Hyde, C. C. (1999) The crystal structure of the SIV gp41 ectodomain at 1.47 Å resolution, *J. Struct. Biol.* 126, 131–144.
 32. Chen, J., Skehel, J. J., and Wiley, D. C. (1999) N- and C-terminal residues combine in the fusion-pH influenza hemagglutinin HA₂ subunit to form an N cap that terminates the triple-stranded coiled coil, *Proc. Natl. Acad. Sci. U.S.A.* 96, 8967–8972.
 33. Carr, C. M., and Kim, P. S. (1993) A spring-loaded mechanism for the conformational change of influenza hemagglutinin, *Cell* 73, 823–832.
 34. Wilson, I. A., Skehel, J. J., and Wiley, D. C. (1981) Structure of the haemagglutinin membrane glycoprotein of influenza virus at 3 Å resolution, *Nature* 289, 366–373.
 35. Bentz, J. (2000) Membrane fusion mediated by coiled coils: a hypothesis, *Biophys. J.* 78, 886–900.
 36. Bentz, J. (2000) Minimal aggregate size and minimal fusion unit for the first fusion pore of influenza hemagglutinin-mediated membrane fusion, *Biophys. J.* 78, 227–245.
 37. Kang, C. Y., Hariharan, K., Nara, P. L., Sodroski, J., and Moore, J. P. (1994) Immunization with a soluble CD4–gp120 complex preferentially induces neutralizing anti-human immunodeficiency virus type 1 antibodies directed to conformation-dependent epitopes of gp120, *J. Virol.* 68, 5854–5862.
 38. Kwong, P. D., Wyatt, R., Robinson, J., Sweet, R. W., Sodroski, J., and Hendrickson, W. A. (1998) Structure of an HIV gp120 envelope glycoprotein in complex with the CD4 receptor and a neutralizing human antibody, *Nature* 393, 648–659.
 39. Munoz-Barroso, I., Durell, S., Sakaguchi, K., Appella, E., and Blumenthal, R. (1998) Dilation of the human immunodeficiency virus-1 envelope glycoprotein fusion pore revealed by the inhibitory action of a synthetic peptide from gp41, *J. Cell Biol.* 140, 315–323.
 40. Chang, D. K., Cheng, S. F., and Chien, W. J. (1997) The amino-terminal fusion domain peptide of human immunodeficiency virus type 1 gp41 inserts into the sodium dodecyl sulfate micelle primarily as a helix with a conserved glycine at the micelle–water interface, *J. Virol.* 71, 6593–6602.
 41. Glaser, R. W., Grune, M., Wandelt, C., and Ulrich, A. S. (1999) Structure analysis of a fusogenic peptide sequence from the sea urchin fertilization protein bindin, *Biochemistry* 38, 2560–2569.
 42. Curtain, C., Separovic, F., Nielsen, K., Craik, D., Zhong, Y., and Kirkpatrick, A. (1999) The interactions of the N-terminal fusogenic peptide of HIV-1 gp41 with neutral phospholipids, *Eur. Biophys. J.* 28, 427–436.
 43. Bradshaw, J. P., Darkes, M. J., Harroun, T. A., Katsaras, J., and Epand, R. M. (2000) Oblique membrane insertion of viral fusion peptide probed by neutron diffraction, *Biochemistry* 39, 6581–6585.
 44. Taylor, S. E., Desbat, B., Blaudez, D., Jacobi, S., Chi, L. F., Fuchs, H., and Schwarz, G. (2000) Structure of a fusion peptide analogue at the air–water interface, determined from surface activity, infrared spectroscopy, and scanning force microscopy, *Biophys. Chem.* 87, 63–72.
 45. Han, X., and Tamm, L. K. (2000) pH-dependent self-association of influenza hemagglutinin fusion peptides in lipid bilayers, *J. Mol. Biol.* 304, 953–965.
 46. Yang, J., Gabrys, C. M., and Weliky, D. P. (2001) Solid-state nuclear magnetic resonance evidence for an extended beta strand conformation of the membrane-bound HIV-1 fusion peptide, *Biochemistry* 40, 8126–8137.
 47. Han, X., Bushweller, J. H., Cafiso, D. S., and Tamm, L. K. (2001) Membrane structure and fusion-triggering conformational change of the fusion domain from influenza hemagglutinin, *Nat. Struct. Biol.* 8, 715–720.
 48. Epand, R. M., Epand, R. F., Martin, I., and Ruyschaert, J. M. (2001) Membrane interactions of mutated forms of the influenza fusion peptide, *Biochemistry* 40, 8800–8807.
 49. Hsu, C. H., Wu, S. H., Chang, D. K., and Chen, C. P. (2002) Structural characterizations of fusion peptide analogues of influenza virus hemagglutinin—Implication of the necessity of a helix–hinge–helix motif in fusion activity, *J. Biol. Chem.* 277, 22725–22733.
 50. Gordon, L. M., Mobley, P. W., Pilpa, R., Sherman, M. A., and Waring, A. J. (2002) Conformational mapping of the N-terminal peptide of HIV-1 gp41 in membrane environments using C-13-enhanced Fourier transform infrared spectroscopy, *Biochim. Biophys. Acta* 1559, 96–120.
 51. Saez-Cirion, A., and Nieva, J. L. (2002) Conformational transitions of membrane-bound HIV-1 fusion peptide, *Biochim. Biophys. Acta* 1564, 57–65.
 52. Yang, J., Parkanzky, P. D., Bodner, M. L., Duskin, C. G., and Weliky, D. P. (2002) Application of REDOR subtraction for filtered MAS observation of labeled backbone carbons of membrane-bound fusion peptides, *J. Magn. Reson.* 159, 101–110.
 53. Kim, C. H., Macosko, J. C., Yu, Y. G., and Shin, Y. K. (1996) On the dynamics and confirmation of the HA₂ domain of the influenza virus hemagglutinin, *Biochemistry* 35, 5359–5365.
 54. Macosko, J. C., Kim, C. H., and Shin, Y. K. (1997) The membrane topology of the fusion peptide region of influenza hemagglutinin determined by spin-labeling EPR, *J. Mol. Biol.* 267, 1139–1148.
 55. Kim, C. H., Macosko, J. C., and Shin, Y. K. (1998) The mechanism for low-pH-induced clustering of phospholipid vesicles carrying the HA₂ ectodomain of influenza hemagglutinin, *Biochemistry* 37, 137–144.
 56. LeDuc, D. L., Shin, Y. K., Epand, R. F., and Epand, R. M. (2000) Factors determining vesicular lipid mixing induced by shortened constructs of influenza hemagglutinin, *Biochemistry* 39, 2733–2739.
 57. Leikina, E., LeDuc, D. L., Macosko, J. C., Epand, R., Shin, Y. K., and Chernomordik, L. V. (2001) The 1–127 HA₂ construct of influenza virus hemagglutinin induces cell–cell hemifusion, *Biochemistry* 40, 8378–8386.
 58. Epand, R. F., Yip, C. M., Chernomordik, L. V., LeDuc, D. L., Shin, Y. K., and Epand, R. M. (2001) Self-assembly of influenza hemagglutinin: studies of ectodomain aggregation by in situ atomic force microscopy, *Biochim. Biophys. Acta* 1513, 167–175.

59. Han, X., and Tamm, L. K. (2000) A host-guest system to study structure-function relationships of membrane fusion peptides, *Proc. Natl. Acad. Sci. U.S.A.* *97*, 13097-13102.
60. Aloia, R. C., Tian, H., and Jensen, F. C. (1993) Lipid composition and fluidity of the human immunodeficiency virus envelope and host cell plasma membranes, *Proc. Natl. Acad. Sci. U.S.A.* *90*, 5181-5185.
61. Hope, M. J., Bally, M. B., Webb, G., and Cullis, P. R. (1985) Production of large unilamellar vesicles by a rapid extrusion procedure—Characterization of size distribution, trapped volume, and ability to maintain a membrane-potential, *Biochim. Biophys. Acta* *812*, 55-65.
62. Struck, D. K., Hoekstra, D., and Pagano, R. E. (1981) Use of resonance energy transfer to monitor membrane fusion, *Biochemistry* *20*, 4093-4099.
63. Gullion, T., and Schaefer, J. (1989) Rotational-echo double-resonance NMR, *J. Magn. Reson.* *81*, 196-200.
64. Bennett, A. E., Rienstra, C. M., Auger, M., Lakshmi, K. V., and Griffin, R. G. (1995) Heteronuclear decoupling in rotating solids, *J. Chem. Phys.* *103*, 6951-6958.
65. Gullion, T., Baker, D. B., and Conradi, M. S. (1990) New, compensated Carr-Purcell sequences, *J. Magn. Reson.* *89*, 479-484.
66. Gullion, T., and Schaefer, J. (1991) Elimination of resonance offset effects in rotational-echo, double-resonance NMR, *J. Magn. Reson.* *92*, 439-442.
67. Wishart, D. S., Sykes, B. D., and Richards, F. M. (1991) Relationship between nuclear magnetic resonance chemical shift and protein secondary structure, *J. Mol. Biol.* *222*, 311-333.
68. Chang, D. K., Cheng, S. F., and Trivedi, V. D. (1999) Biophysical characterization of the structure of the amino-terminal region of gp41 of HIV-1. Implications on viral fusion mechanism, *J. Biol. Chem.* *274*, 5299-5309.
69. Yang, J., and Weliky, D. P., unpublished experiments.
70. Lloyd-Williams, P., Albericio, F., and Giralt, E. (1997) *Chemical Approaches to the Synthesis of Peptides and Proteins*, CRC, Boca Raton, FL.
71. Parkanzky, P. D., and Weliky, D. P., unpublished experiments.

BI027052G